2015 American Control Conference
Palmer House Hilton
July 1-3, 2015. Chicago, IL, USA

Retrospective Cost Adaptive Thrust Control of a 1D scramjet with Mach Number Disturbance

Ankit Goel[1], Antai Xie[2], Karthik Duraisamy[3], and Dennis S. Bernstein[4]

Abstract— **We use retrospective cost adaptive control (RCAC) to control the thrust generated by a scramjet. A quasi-one-dimensional version of the mass, momentum, and energy conservation equations of compressible fluid flow with heat release is used to model the physics of the scramjet. First, we study the dynamic behavior of the scramjet model. Then, we apply system identification techniques to fit a linear model to the data generated by the scramjet model to investigate the dependence of scramjet dynamics on the Mach number. Finally, we use RCAC to maintain the commanded thrust in the presence of a disturbance in the Mach number.**

I. Introduction

A scramjet (supersonic combustion ramjet) engine is an airbreathing propulsion system that has demonstrated potential for high-speed transport, access to space, and payload delivery [1]. A scramjet engine compresses and ignites a supersonic stream of air and generates thrust by accelerating high-energy air through a nozzle. This process is achieved without moving parts.

A complicating factor in the design of a scramjet vehicle stems from the requirement to maintain flow conditions inside the engine within a narrow range of acceptable limits. Crossing any of these limits, which are dictated by thermodynamics and fluid mechanics, can lead to instabilities that could result in catastrophic failure of the vehicle. The ability to control the internal flow conditions and maintain the system thrust in the presence of external disturbances is thus of great technological value.

In this paper, we apply retrospective cost adaptive control (RCAC) [2] to the problem of controlling the simulated generated thrust of a scramjet model. A quasi-one-dimensional version of the mass, momentum, and energy conservation equations of compressible fluid flow is used to model the physics of the scramjet. The scramjet model is developed as a computational fluid dynamics code.

We study two control problems in this paper. The first is to have the thrust output to follow a commanded value, and the second is to maintain the thrust output at a reference value in the presence of disturbances in operating conditions. A key difficulty in the second problem arises from the fact that the dynamics depend on the disturbance.

II. Scramjet model

We consider a scramjet model based on the Hyshot vehicle built and tested by the University of Queensland over the past two decades [1]. The relevant physics are assumed to be governed by the quasi-one-dimensional Euler equations of gas dynamics supplemented with a heat-release model [3], [4] to represent the effect of fuel-injection and ignition. These equations are given by

$$\frac{\partial}{\partial t}\begin{bmatrix}\rho A\\ \rho u A\\ eA\end{bmatrix}+\frac{\partial}{\partial x}\begin{bmatrix}\rho u A\\ (\rho u^2+p)A\\ u(e+p)A\end{bmatrix}=\begin{bmatrix}0\\ p\frac{\partial A}{\partial x}\\ \dot{q}\end{bmatrix} \quad (1)$$

where, ρ, u, p are the fluid density, velocity and pressure. The total energy per unit volume e can be written in terms of the velocity and pressure as

$$e=\frac{p}{\gamma-1}+\frac{1}{2}\rho u^2, \quad (2)$$

where γ is the ratio of specific heats. A is the cross-sectional area of the scramjet and $\dot{q}$ is the heat release during the combustion, which is assumed to be directly proportional to the fuel-injection rate. These equations have a hyperbolic character in time, and the flow variables can include discontinuous profile changes in space and time because of the presence of shock wave. Spatial discretization using 150 equally spaced axial stations leads to a set of 450 coupled nonlinear ordinary differential equations, which are integrated using a fourth-order Runge-Kutta method.

The variation of the cross-sectional area with the axial distance from the inlet of the scramjet used in this paper is shown in Figure 1a. The initial constant area section corresponds to the isolator region; the first linear variation represents the combustor, and the second linear variation represents the nozzle. A steady-state solution is sought for a nominal operating condition of the scramjet, an example of which is shown in Figure 1b. In the present setup, "operating condition" corresponds to the flight speed (represented by the Mach number at the inlet of the scramjet). Control is applied by increasing or decreasing the fuel-injection rate which affects the heat release of combustion. The system thrust is determined by computing a momentum balance between the inlet plane and the exit plane of the scramjet.

III. RCAC Algorithm

A. Plant Model

Consider the MIMO discrete-time system

$$x(k+1)=Ax(k)+Bu(k)+D_1w(k), \quad (3)$$

$$y(k)=Cx(k)+D_2w(k), \quad (4)$$

$$z(k)=E_1x(k)+E_0w(k), \quad (5)$$

where $x(k)\in\mathbb{R}^{l_x}$ is the state, $y(k)\in\mathbb{R}^{l_y}$ is the measurement, $u(k)\in\mathbb{R}^{l_u}$ is the input, $w(k)\in\mathbb{R}^{l_w}$ is the exogenous

[1]Ankit Goel and [2]Antai Xie are graduate students with Department of Aerospace Engineering, University of Michigan, Ann Arbor, MI 48109, USA ankgoel@umich.edu, antai@umich.edu

[3]Karthik Duraisamy and [4]Dennis S. Bernstein are with faculty of Aerospace Engineering, University of Michigan, Ann Arbor, MI 48109, USA kdur@umich.edu, dsbaero@umich.edu

978-1-4799-8686-6/$31.00 ©2015 AACC

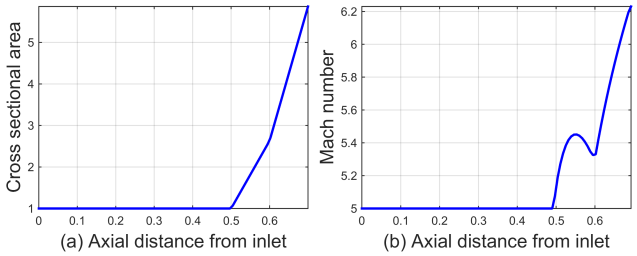

Fig. 1: (a) shows the cross sectional area normalized by the inlet area. The first linear variation is due to the combustor, and the second linear variation is due to the nozzle. (b) shows an illustrative steady-state axial Mach number profile.

signal, and $z(k) \in \mathbb{R}^{l_z}$ is the performance variable. The goal is to develop an adaptive output feedback controller that minimizes z in the presence of the exogenous signal w with limited modeling information about (3)–(5). The components of w can represent either command signals to be followed, external disturbances to be rejected, or both, depending on the choice of D_1 and E_0. This formulation defines the signals that play a role in RCAC. However, no assumptions are made concerning the state space realization since RCAC requires only input-output model information.

B. The Controller

Define the dynamic compensator

$$u(k) = \sum_{i=1}^{n_c} M_i(k)u(k-i) + \sum_{i=k_0}^{n_c} N_i(k)\xi(k-i), \tag{6}$$

where $M_i(k) \in \mathbb{R}^{l_u \times l_u}$, $N_i(k) \in \mathbb{R}^{l_u \times l_\xi}$ are the controller coefficient matrices, $k_0 \geq 0$, and $\xi(k) \in \mathbb{R}^{l_\xi}$ consists of components of y, z, and w. We rewrite (6) as

$$u(k) = \Phi(k)\theta(k), \tag{7}$$

where the regressor matrix $\Phi(k)$ is defined by

$$\Phi(k) \triangleq \begin{bmatrix} u(k-1) \\ \vdots \\ u(k-n_c) \\ \xi(k-k_0) \\ \vdots \\ \xi(k-n_c) \end{bmatrix}^{\mathrm{T}} \otimes I_{l_u} \in \mathbb{R}^{l_u \times l_\theta},$$

and

$$\theta(k) \triangleq \mathrm{vec}\begin{bmatrix} M_1(k) \cdots M_{n_c}(k) & N_{k_0}(k) \cdots N_{n_c}(k) \end{bmatrix} \in \mathbb{R}^{l_\theta},$$

where $l_\theta \triangleq l_u^2 n_c + l_u l_\xi (n_c + 1 - k_0)$, "$\otimes$" is the Kronecker product, and "vec" is the column-stacking operator. Note that $k_0 = 0$ yields an exactly proper controller, whereas $k_0 \geq 1$ yields a strictly proper controller.

C. Retrospective Performance Variable

We define the retrospective control as

$$\hat{u}(k) = \Phi(k)\hat{\theta} \tag{8}$$

and the corresponding retrospective performance variable as

$$\hat{z}(k) \triangleq z_{\mathrm{f}}(k) + \Phi_{\mathrm{f}}(k)\hat{\theta} - u_{\mathrm{f}}(k), \tag{9}$$

where $\hat{\theta} \in \mathbb{R}^{l_\theta}$ is determined by optimization below, and $z_{\mathrm{f}}(k) \in \mathbb{R}^{l_z}$, $\Phi_{\mathrm{f}}(k) \in \mathbb{R}^{l_z \times l_\theta}$, and $u_{\mathrm{f}}(k) \in \mathbb{R}^{l_z}$ are filtered versions of $z(k), \Phi(k), u(k)$, respectively, defined by

$$z_{\mathrm{f}}(k) \triangleq G_{\mathrm{f}_z}(\mathbf{q})z(k), \tag{10}$$

$$\Phi_{\mathrm{f}}(k) \triangleq G_{\mathrm{f}_u}(\mathbf{q})\Phi(k). \tag{11}$$

$$u_{\mathrm{f}}(k) \triangleq G_{\mathrm{f}_u}(\mathbf{q})u(k). \tag{12}$$

The filters G_{f_z} and G_{f_u} have the form

$$G_{\mathrm{f}_z}(\mathbf{q}) \triangleq D_z^{-1}(\mathbf{q})N_z(\mathbf{q}), \tag{13}$$

$$G_{\mathrm{f}_u}(\mathbf{q}) \triangleq D_u^{-1}(\mathbf{q})N_u(\mathbf{q}), \tag{14}$$

where D_z, N_z, D_u, and N_u are polynomial matrices, and D_z and D_u are monic.

D. Retrospective Cost Function

Using the retrospective performance variable $\hat{z}(k)$, we define the retrospective cost function

$$J(k,\hat{\theta}) \triangleq \sum_{i=1}^{k} \lambda^{k-i} \left[\hat{z}^{\mathrm{T}}(i)R_z\hat{z}(i) + (\Phi_{\mathrm{f}}(i)\hat{\theta})^{\mathrm{T}}R_{\mathrm{f}}\Phi_{\mathrm{f}}(i)\hat{\theta} \right] + \lambda^k(\hat{\theta} - \theta(0))^{\mathrm{T}}R_\theta(\hat{\theta} - \theta(0)), \tag{15}$$

where R_z and R_θ are positive definite, R_{f} is positive semidefinite, and $\lambda \in (0,1]$ is the forgetting factor.

Proposition: Let $P(0) = R_\theta^{-1}$. Then, for all $k \geq 1$, the retrospective cost function (15) has a unique global minimizer $\theta(k)$, which is given by

$$\theta(k) = \theta(k-1) - P(k-1)\Phi_{\mathrm{f}}^{\mathrm{T}}(k)\Gamma^{-1}(k) \cdot [\Phi_{\mathrm{f}}(k)\theta(k-1) + (R_z + R_{\mathrm{f}})^{-1}R_z(z_{\mathrm{f}}(k) - u_{\mathrm{f}}(k))], \tag{16}$$

$$P(k) = \frac{1}{\lambda}P(k-1) - \frac{1}{\lambda}P(k-1)\Phi_{\mathrm{f}}^{\mathrm{T}}(k)\Gamma^{-1}(k)\Phi_{\mathrm{f}}(k)P(k-1), \tag{17}$$

where

$$\Gamma(k) \triangleq \lambda(R_z + R_{\mathrm{f}})^{-1} + \Phi_{\mathrm{f}}(k)P(k-1)\Phi_{\mathrm{f}}^{\mathrm{T}}(k).$$

IV. Nonlinearity of the Scramjet Dynamics

In this section, we define the operating envelope of the scramjet and analyze the open-loop response of the scramjet model to ascertain the qualitative behavior of its dynamics. The scramjet is a SISO plant, where the input $u(t)$ is the fuel-injection rate, and the output $y(t)$ is the thrust generated by the scramjet. The fuel-injection rate is non-dimensionalized by the air mass flow rate, and the thrust is non-dimensionalized by $\frac{1}{2}\rho_\infty u_\infty \mathrm{L}^2$, where ρ_∞ and u_∞ are the free stream density and velocity, and L is the grid length. The Mach number $M(t) = M_0 + m(t)$ is modeled as the sum of a constant M_0 and a Mach number perturbation $m(t)$. The time step used in the scramjet model is $T_s = 10^{-4}$ sec.

To define the operating envelope, we study the steady-state flow solution. Depending on the inlet Mach number and fuel-injection rate, the flow in the combustor can either

be supersonic or subsonic in normal operation. However, if sufficient heat is added, a normal shock will travel upstream at acoustic velocity. This phenomena is known as Unstart , and is typically fatal for the scramjet. To determine the fuel-injection rate which causes the scramjet to unstart, we look at the steady-state solutions of the flow for various constant Mach numbers and fuel-injection rates. For a given Mach number and fuel-injection rate, if the scramjet unstarts, the flow in the inlet will becomes subsonic. Figure 2 shows the values Mach number and fuel-injection rate corresponding to unstart and normal operation.

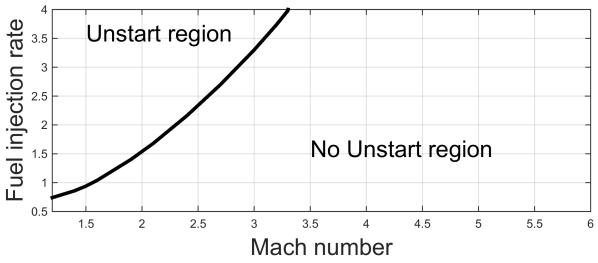

Fig. 2: Operating envelope. The region to the left of the line implies that, for the given Mach number and fuel-injection rate, the flow will choke and the scramjet will unstart.

A. Impulse response

To determine the impulse response of the scramjet, the system is allowed to evolve at a constant Mach number with $u(t) = 0$. The generated thrust $y(t)$ then reaches an asymptotic value by $t = 1$ sec. At $t = 2$ sec, $u(t) = u_0\delta(t-2)$ is applied with $u_0 \in \{1, 2, ..., 7\}$ and constant Mach numbers $M_0 \in \{1, 2, 3, 4\}$. Figure 3 shows the thrust generated for each impulse magnitude and each Mach number. Figure 4 shows the peak value of the impulse response. Note that the peak value increases linearly with u_0.

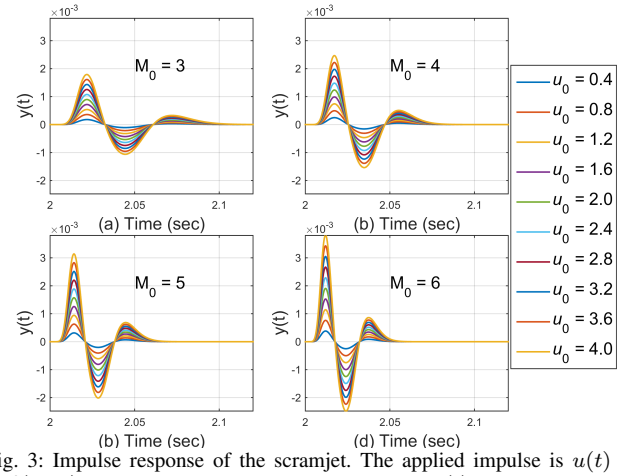

Fig. 3: Impulse response of the scramjet. The applied impulse is $u(t) = u_0\delta(t-2)$. The subplots show the generated thrust $y(t)$ at a constant Mach number $M_0 \in \{3, 4, 5, 6\}$ for $u_0 \in \{0.4, 0.8, ..., 4.0\}$. Note that the DC bias is subtracted from each response.

B. Step response

To determine the step response of the scramjet, the system is allowed to evolve at a constant Mach number with $u(t) = 0$. The thrust $y(t)$ then reaches an asymptotic value by $t = 1$ sec. At $t = 2$ sec, $u(t) = u_0 1(t-2)$ is applied with $u_0 \in \{0.4, 0.8, ..., 4.0\}$ and constant Mach numbers $M_0 \in \{3, 4, 5, 6\}$. Figure 5 shows the generated thrust for each step magnitude and Mach number. Figure 6 shows the asymptotic value of the step response. Note that the asymptotic value does not increase linearly with u_0 as the flow conditions in the combustor change from supersonic to subsonic.

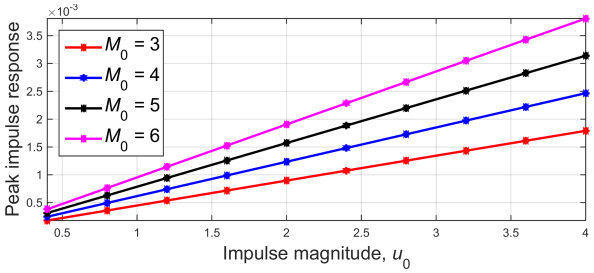

Fig. 4: Peak value of the thrust generated by the scramjet for the impulsive input $u(t) = u_0\delta(t)$ as u_0 is increased from 0.4 to 4.0 at constant Mach number M_0. Note that the peak thrust value increases linearly with u_0 for each Mach number.

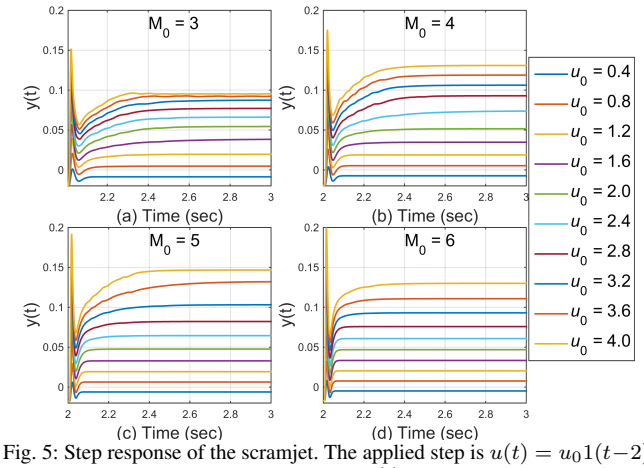

Fig. 5: Step response of the scramjet. The applied step is $u(t) = u_0 1(t-2)$. The subplots show the generated thrust $y(t)$ at a constant Mach number $M_0 \in \{3, 4, 5, 6\}$ for $u_0 \in \{0.4, 0.8, ..., 4.0\}$.

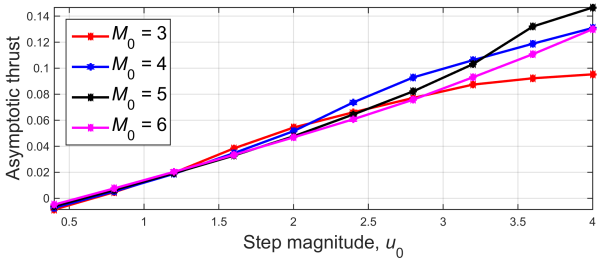

Fig. 6: Asymptotic value of the generated thrust by the scramjet for constant Mach number M_0 subjected to the step input $u(t) = u_0 1(t-2)$ as u_0 increases from 0.4 to 4.0. The plot shows that the asymptotic value of the thrust is a nonlinear function of the step magnitude.

C. Harmonic response

Case IV-C.1. To determine the open-loop response of the scramjet to a harmonic fuel-injection rate, the system is allowed to evolve at a constant Mach number $M_0 \equiv 3$ and fuel-injection rate $u(t) \equiv 2$. The generated thrust $y(t)$ then reaches an asymptotic value by $t = 1$ sec. At $t = 1.5$ sec, fuel-injection rate $u(t) = 2 + \sin(6\pi t)$ is applied. The open-loop response of the scramjet is shown in Figure 7.

Case IV-C.2. To determine the open-loop response of scramjet to a harmonic Mach number, the system is allowed to evolve at the constant Mach number $M_0 = 3$ and fuel-injection rate $u(t) \equiv 2$. The generated thrust $y(t)$ then

reaches an asymptotic value by $t = 1$ sec. At $t = 1.5$ sec, the Mach number is varied as $M(t) = 3 + \sin(6\pi t)$. The open-loop response of the scramjet is shown in Figure 8.

Figure 9 shows the frequency spectrum of the open-loop response in **Case IV-C.1** and **Case IV-C.2**. The appearance of spectral content in the thrust output not present in the input indicates that the scramjet dynamics are nonlinear.

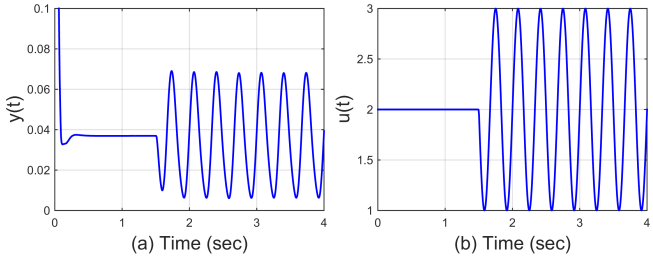

Fig. 7: **Case IV-C.1**. Open-loop response of the scramjet. The input is $u(t) = 2+\sin(6\pi t)$ for $t > 1.5$ and the constant Mach number is $M_0 = 3$. (a) shows the thrust $y(t)$ generated by the scramjet. (b) shows the fuel-injection rate $u(t)$ applied to the scramjet.

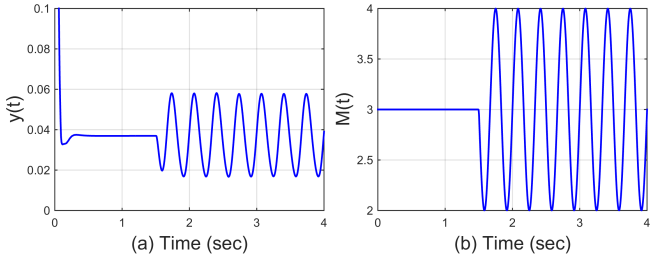

Fig. 8: **Case IV-C.2**. Open-loop response of the scramjet. The input is $u(t) \equiv 2$ and the Mach number is $M(t) = 3 + \sin(6\pi t)$ for $t > 1.5$. (a) shows the thrust $y(t)$ generated by the scramjet. (b) shows the disturbance in the Mach number.

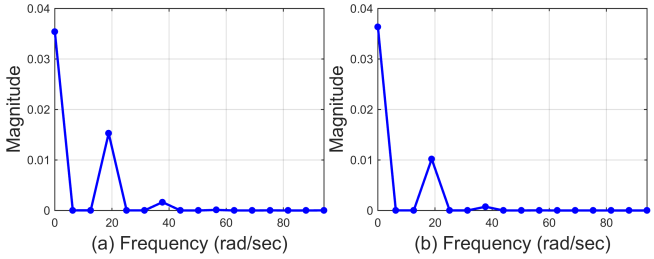

Fig. 9: (a) **Case IV-C.1**. Magnitudes of the harmonics present in the thrust output for harmonic input and constant Mach number. (b) **Case IV-C.2**. Magnitudes of the harmonics present in the output for constant input and harmonic Mach number. The presence of multiple harmonics in the output shows the nonlinearity of the scramjet model.

V. Linear Identification of the Scramjet Dynamics

In this section, we use the impulse response of the scramjet to construct a transfer function that approximates the impulse response. The impulse response sequence is generated by applying the unit-magnitude impulse $u(t) = \delta(t - 2)$ for constant Mach numbers $M_0 \in \{3, 4, 5, 6\}$. We remove the DC bias from the impulse response, as shown in Figure 10. Note that the impulse response changes as the Mach number changes.

We use the Hankel matrix rank test and nuclear norm minimization [5], [6] to estimate the transfer function order. The impulse response sequence is down-sampled by selecting every 50^{th} sample, hence the sampling time becomes $T_s = 0.005$ sec. Figure 11 shows the singular values of the Hankel matrix constructed from the downsampled impulse response. Using the Hankel matrix test, we conclude that the order decreases as the Mach number increases. As shown in Figure 12, the nuclear norm minimization test also suggests the order to be Mach number dependednt.

We apply ERA [7] to construct transfer functions of the order suggested by nuclear norm minimization for each Mach number. The pole-zero maps of the transfer functions thus obtained are shown in Figure 13. Note that the poles move closer to origin as the Mach number increases. Bode plots of the four transfer functions are shown in Figure 14.

From the impulse response of the scramjet, the pole-zero map, and the bode plots of the approximated transfer functions , we conclude that the scramjet dynamics depend on the Mach number.

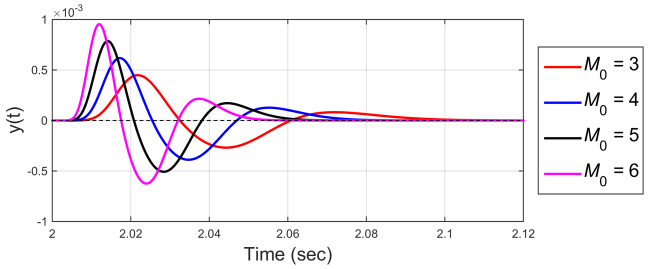

Fig. 10: Impulse response of scramjet for constant Mach numbers $M_0 \in \{3, 4, 5, 6\}$. The scramjet model is allowed to reach a steady-state with $u(t) = 0$. At $t = 2$ sec, unit-magnitude impulse $u(t) = \delta(t - 2)$ is applied. The impulse response shows that the generated thrust is Mach number dependent.

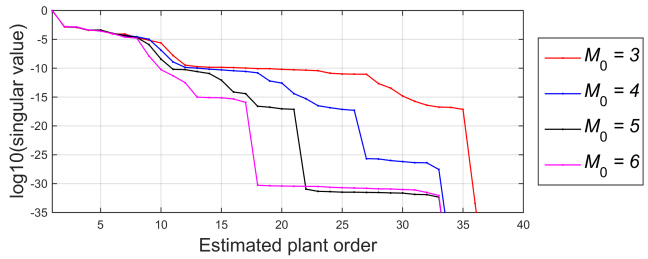

Fig. 11: Singular values of the Hankel matrix constructed from the impulse response. The drop in singular values suggests that the order of the transfer function that best approximates the impulse response of the scramjet.

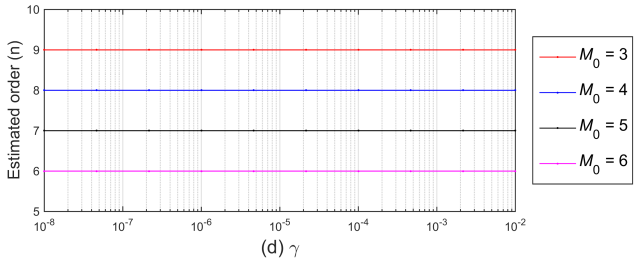

Fig. 12: Estimated transfer function order using nuclear norm minimization algorithm. The magnitude γ of perturbation in the impulse response, increases from 10^{-8} to 10^{-2} logarithmically. The results suggest that the system order depends on Mach number.

VI. Closed-loop Response of the Scramjet

In this section, we present command following and disturbance rejection results with RCAC for the scramjet model.

Although RCAC is developed for linear systems. it has been shown to be useful for nonlinear plants [8]. To implement RCAC, we define the performance variable $z(t)$ as the difference between the thrust output $y(t)$ of the scramjet

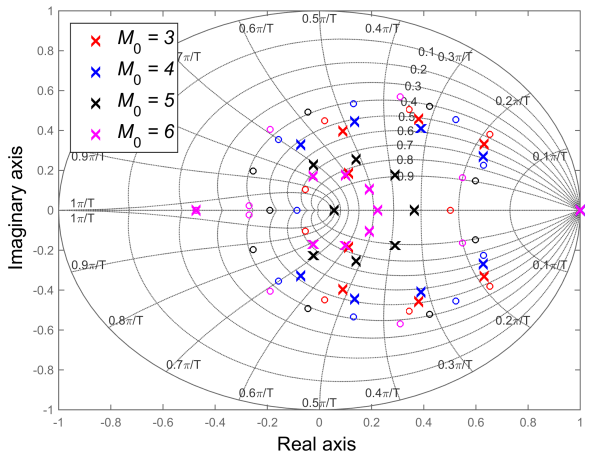

Fig. 13: Pole-zero map of the transfer functions constructed using ERA from the impulse response at four Mach numbers. Note that the poles and zeros of the approximated transfer function change as M changes.

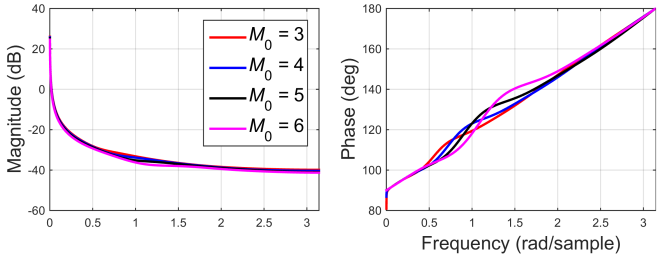

Fig. 14: Bode plots of the transfer functions constructed using ERA from the impulse response at constant Mach number $M_0 \in \{3, 4, 5, 6\}$.

and the thrust command $r(t)$, that is, $z(t) = y(t) - r(t)$. The fuel-injection rate $u(t)$, is controlled by RCAC. In this case, $z(t), u(t)$ and $r(t)$ are scalars.

RCAC is a discrete-time controller that operates at a constant sample time. To use RCAC with the scramjet model, we fix the time step as $T_s = 10^{-4}$ sec. The continuous time variable t and the discrete time variable k are related as $t = kT_s$. Constant fuel-injection rate $u(t) = 1$ is used to allow the scramjet model to reach steady-state before RCAC is switched on at $t = 1.5$ sec. To avoid excessive transients, we saturate the RCAC output $u(t)$ over the interval $1 \leq u(t) \leq 7$.

In the following results, we set $R_z = 1, R_{\mathrm{f}} = 0$, use the filters $G_{\mathrm{f}_z}(\mathbf{q}) = G_{\mathrm{f}_u}(\mathbf{q}) = 1$, which captures sign information, and $n_c = 35$. No other modeling information is used from the scramjet model.

A. Command following

Case VI-A.1. [*Setpoint command following*] The commanded thrust is 0.04. At $t = 3$ sec, the command $r(t)$ is changed to 0.03. At $t = 4.5$ sec, the command $r(t)$ is changed to 0.05. The constant Mach number is $M_0 \equiv 2$. RCAC tuning parameters are $P_0 = 100I$ and $\lambda = 1$. The closed-loop response is shown in Figure 15.

Case VI-A.2. [*Harmonic command following*] The command is $r(t) = 0.04 + 0.01\sin(6\pi t)$ and the constant Mach number $M_0 \equiv 2$. RCAC tuning parameters are $P_0 = 100I$ and $\lambda = 1$. The closed-loop response is shown in Figure 16.

B. Disturbance Rejection

Case VI-B.1. [*Step disturbance*.] The thrust command $r(t) \equiv 0.04$ and the Mach number $M(t) = 2$ for $t \in [0, 3)$, $M(t) = 3$ for $t \in [3, 4.5)$, and $M(t) = 4$ for $t \in [4.5, 6)$. RCAC tuning parameters are $P_0 = 100I$ and $\lambda = 1$. The closed-loop response is shown in Figure 17.

Case VI-B.2. [*Harmonic disturbance*] The thrust command $r(t) \equiv 0.04$ and the Mach number is $M(t) = 2 + 0.02\sin(6\pi t)$. RCAC tuning parameters are $P_0 = 1I$ and $\lambda = 0.99$. The closed-loop response is shown in Figure 18.

Case VI-B.3. [*Harmonic disturbance*] The thrust command $r(t) \equiv 0.04$, the Mach number is $M(t) = 2 + 0.1\sin(6\pi t)$. RCAC tuning parameters are $P_0 = 1I$ and $\lambda = 0.99$. The closed-loop response is shown in Figure 19.

Case VI-B.4. [*Harmonic disturbance*] The thrust command $r(t) \equiv 0.04$, the Mach number is $M(t) = 2 + 0.2\sin(6\pi t)$. RCAC tuning parameters are $P_0 = 1I$ and $\lambda = 0.99$. The closed-loop response is shown in Figure 20.

C. Harmonic command following with harmonic disturbance

Case VI-C.1. [*Harmonic command with harmonic disturbance*] The thrust command is $r(t) = 0.04 + 0.01\sin(1.5\pi t)$ and the Mach number is $M(t) = 2 + 0.05\sin(6\pi t)$. RCAC tuning parameters are $P_0 = 1I$ and $\lambda = 0.999$. The closed-loop response is shown in Figure 21.

Case VI-C.2. [*Harmonic command with harmonic disturbance*] The thrust command is $r(t) = 0.04 + 0.01\sin(6\pi t)$ and the Mach number is $M(t) = 2 + 0.05\sin(6\pi t)$. RCAC tuning parameters are $P_0 = 1I$ and $\lambda = 0.999$. The closed-loop response is shown in Figure 22.

VII. Conclusion

In this paper, we applied retrospective cost adaptive control (RCAC) to thrust control for a 1D scramjet model. Thrust command following and Mach number disturbance rejection were considered for both step and harmonic commands and disturbances. Using system identification techniques, the scramjet dynamics were shown to be nonlinear and Mach number dependent. Aside from sign information, RCAC required no modeling information from the scramjet model. Simulation results showed that RCAC is able to follow and maintain the commanded thrust when the Mach number is constant. In cases where the Mach number has a harmonic perturbation, RCAC reduced the amplitude of the disturbance in the thrust generated by an order of magnitude as compared to the open-loop case. Finally, RCAC uses only limited input-output modeling information and thus treats the dynamics of the system as a black box, which tends to facilitate complex flow problems.

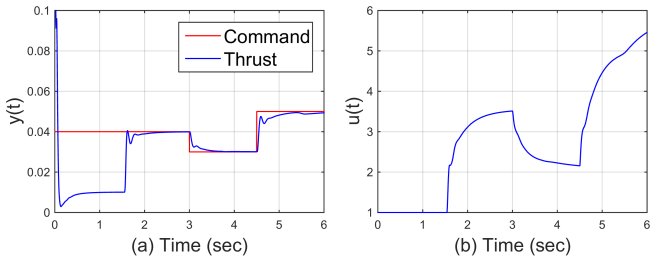

Fig. 15: **Case VI-A.1**. Closed-loop response of the scramjet to a step thrust command. (a) shows the thrust $y(t)$ generated by the scramjet for the thrust command $r(t) = 0.04$ for $t \in [0, 3)$, $r(t) = 0.03$ for $t \in [3, 4.5)$, and $r(t) = 0.05$ for $t \in [4.5, 6)$ and the constant Mach number $M_0 \equiv 2$. (b) shows the fuel-injection rate $u(t)$.

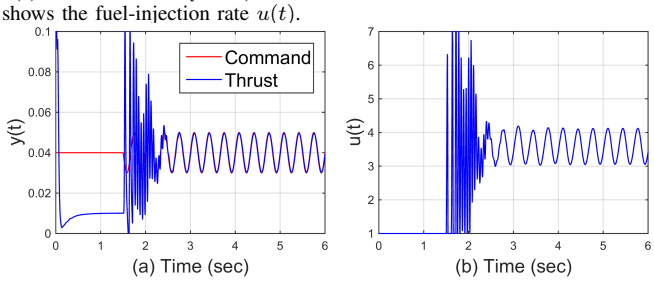

Fig. 16: **Case VI-A.2**. Closed-loop response of the scramjet to a harmonic thrust command. (a) shows the thrust $y(t)$ generated by the scramjet for the thrust command $r(t) = 0.04 + 0.01\sin(6\pi t)$ and the constant Mach number $M_0 \equiv 2$. (b) shows the fuel-injection rate $u(t)$.

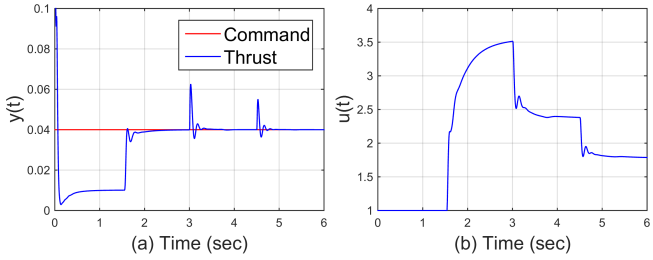

Fig. 17: **Case VI-B.1**. Closed-loop response of the scramjet to a step command in the presence of step disturbances in the Mach number. (a) shows the thrust $y(t)$ generated by the scramjet for the Mach number $M(t) = 2$ for $t \in [0, 3)$, $M(t) = 3$ for $t \in [3, 4.5)$, and $M(t) = 4$ for $t \in [4.5, 6)$.. (b) shows the fuel-injection rate $u(t)$.

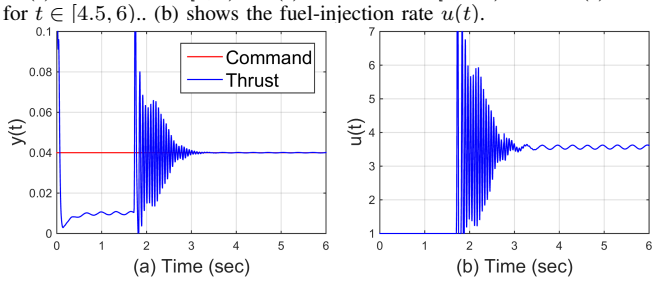

Fig. 18: **Case VI-B.2**. Closed-loop response of the scramjet to a step command in the presence of a harmonic perturbation in the Mach number. (a) shows the thrust $y(t)$ generated by the scramjet for $M(t) = 2 + 0.02\sin(6\pi t)$. (b) shows the fuel-injection rate $u(t)$.

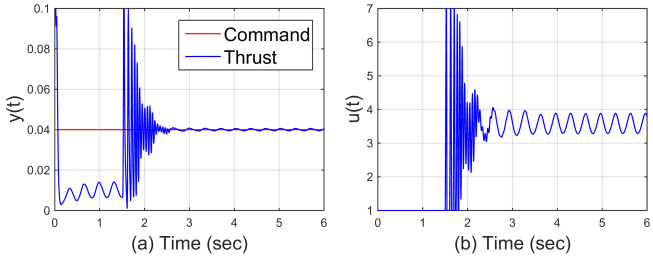

Fig. 19: **Case VI-B.3**. Closed-loop response of the scramjet to a step command in the presence of a harmonic perturbation in the Mach number. (a) shows the thrust $y(t)$ generated by the scramjet for $M(t) = 2 + 0.1\sin(6\pi t)$. (b) shows the fuel-injection rate $u(t)$.

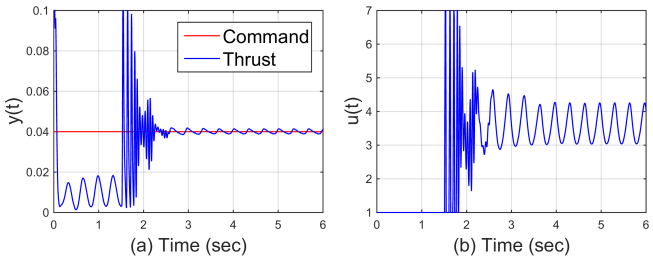

Fig. 20: **Case VI-B.4**. Closed-loop response of the scramjet to a step command in the presence of a harmonic perturbation in the Mach number. (a) shows the thrust $y(t)$ generated by the scramjet for $M(t) = 2 + 0.2\sin(6\pi t)$. (b) shows the fuel-injection rate $u(t)$.

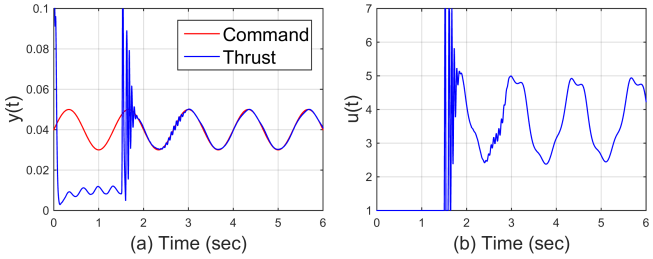

Fig. 21: **Case VI-C.1**. Closed-loop response of the scramjet to a harmonic command in the presence of a harmonic disturbance in the Mach number. The command is $r(t) = 0.04 + 0.01\sin(1.5\pi t)$, and the Mach number is $M(t) = 2 + 0.05\sin(6\pi t)$. (a) shows the thrust $y(t)$ generated by the scramjet. (b) shows the fuel-injection rate $u(t)$.

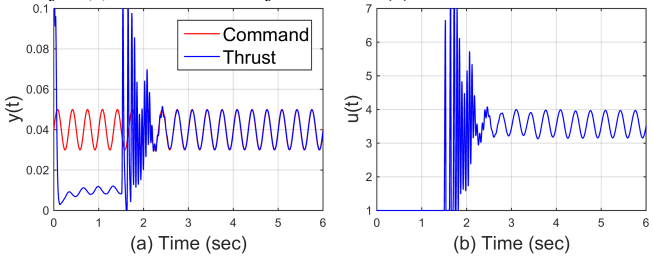

Fig. 22: **Case VI-C.2**. Closed-loop response of the scramjet to a harmonic command in the presence of a harmonic disturbance in the Mach number. The command is $r(t) = 0.04 + 0.01\sin(6\pi t)$, and the Mach number $M(t) = 2 + 0.05\sin(6\pi t)$. (a) shows the thrust $y(t)$ generated by the scramjet. (b) shows the fuel-injection rate $u(t)$.

REFERENCES

[1] M. Smart, N. Hass, and A. Paull, "Flight data analysis of the hyshot 2 scramjet flight experiment," *AIAA Journal*, vol. 44, pp. 2366–2375, 2006.

[2] M. A. Santillo and D. S. Bernstein, "Adaptive Control Based on Retrospective Cost Optimization," *Journal of Guidance, Control, and Dynamics*, vol. 33, pp. 289–304, 2010.

[3] C. Doolan and R. Boyce, "A quasi-one-dimensional mixing and combustion code for trajectory optimisation and design studies," in *AIAA International Space Planes and Hypersonic Systems and Technologies Conference*, no. AIAA 2008-2603, Dayton, Ohio, 2008, pp. 898–907.

[4] Q. Wang, K. Duraisamy, J. Alonso, and G. Iaccarino, "Risk assessment of hypersonic flow simulations using adjoint- based sampling methods," *AIAA Journal*, vol. 50, no. 3, pp. 581–592, April 2012.

[5] R. S. Smith, "Nuclear norm minimization methods for frequency domain subspace identification," in *Proc. American Control Conference*, Montral, Canada, June 2012, pp. 2689–2694.

[6] B. Recht, M. Fazel, and P. A. Parrilo, "Guaranteed minimum-rank solutions of linear matrix equations via nuclear norm minimization," *SIAM Review*, vol. 52(3), pp. 471–501, 2010.

[7] J.-N. Juang, *Applied System Identification*. Upper Saddle River, NJ: Prentice-Hall, 1993.

[8] J. Yan and D. S. Bernstein, "Minimal modeling retrospective cost adaptive control of uncertain hammerstein systems using auxiliary nonlinearities," *Int. J. Contr.*, vol. 87, pp. 483–505, 2014.